

# **A tissue-inspired amorphous photonic metamaterial**

Dapeng Bi

Center for Studies in Physics and Biology, Rockefeller University, NY 10065,USA

## **Abstract**

Inspired by how cells pack in dense biological tissues, we design an amorphous material which possesses a complete photonic band gap. A physical parameter inspired by how cells adhere with one another and regulate their shapes can continuously tune the photonic band gap size as well as the bulk mechanical property of the material. The material can be further tuned to undergo a solid-fluid phase transition during which the shear modulus vanishes yet the photonic band gap persists, hence giving rise to a photonic fluid that is robust to flow and rearrangements. Experimentally this design should lead to the engineering of self-assembled non-rigid photonic structures with photonic band gaps that can be controlled in real time.

Since their introduction [1, 2], Photonic band gap (PBG) materials have remained an intense area of research and has given rise to a wide range of applications such as radiation sources [3], sensors, wave guides, solar arrays and optical computer chips [4]. In particular, many studies have devoted to the design and optimization of photonic crystals – a periodic arrangement of dielectric scattering materials that give rise to photonic bands due to multiple Bragg scatterings. However periodicity is not necessary to form PBGs and amorphous structures with PBGs [5, 6] can offer many advantages over their crystalline counterparts [5]. For example amorphous photonic materials can exhibit band gaps that are directionally isotropic [7, 8] and are also more robust to defects and errors in fabrication [5].

Currently there are two existing protocols for designing amorphous photonic materials. The first is based on structures obtained from a dense packing of spheres [9–12]. The second is a tailor-designed protocol [7, 8, 12] that generates hyperuniform [13] patterns. While these model designs can yield PBGs, the resulting structures cannot be easily self-assembled and are typically static, rigid constructions that do not allow tuning of photonic properties in real time and are unstable to structural changes such as large scale flows and positional rearrangements.

In this work, we propose a new design for amorphous 2D PBG materials that is inspired by how cells pack in dense epithelial tissues. We generate structures that exhibit broad PBGs based on a simple model that has been shown to describe cell shapes and tissue mechanical behavior. An advantage of this design is that the photonic and mechanical properties of the material are closely coupled and can be simultaneously tuned via a single physical parameter. The material can also be tuned to undergo a density-independent solid-fluid transition and the PBG persists well into the fluid phase. With recent advances in tunable self-assembly of nanoparticles or biomimetic emulsion droplets, this design can be used to create a ‘photonic fluid’ with a wide PBG that is robust to flow, perturbations and rearrangements.

When epithelial and endothelial cells pack densely in 2D to form a confluent monolayer, they form a tissue that is well described by a polygonal tiling [14]. The individual cell shapes in the tissue are determined from the mechanics of cell-cell interactions and interaction between cell and the surrounding environment. Recently, a theoretical framework called the Self-Propelled Voronoi (SPV) model has been constructed to understand the precise connection between cell and tissue level mechanics and observed cell shapes in experiments [15, 16]. In the SPV model, the basic degrees of freedom are the set of cell center positions  $\{\mathbf{r}_i\}$  and cell shapes are given by its Voronoi tessellation. The complex biomechanics that govern intracellular and intercellular interactions can

be coarse-grained [14, 15, 17–21] and expressed in terms of an mechanical energy functional for individual cell shapes. For a multicellular tissue given by a collection of cell areas ( $\{A_i\}$ ) and cell perimeters ( $\{P_i\}$ ), the energy functional is given by

$$E = \sum_{i=1}^N [K_A(A_i - A_0)^2 + K_P(P_i - P_0)^2]. \quad (1)$$

The quadratic area term in equation (1) accounts for a cell's resistance to volume changes via an area elastic modulus of  $K_A$  and a homeostatically preferred cell area  $A_0$  [18]. Changes to a cell's perimeter are directly related to the deformation of the acto-myosin cortex concentrated near the cell membrane. In equation (1), the term  $K_P P_i^2$  corresponds to the elastic energy associated with deforming the cortex. The linear term in cell perimeter,  $-K_0 P_0 P_i$ , represents the effective line tension in the cortex and gives rise to a 'preferred perimeter'  $P_0$ . The value of  $P_0$  can be decreased by up-regulating the contractile tension in the cortex [15, 18, 19] and it can be increased by up-regulating cell-cell adhesion. In this work we focus on the properties of the ground states of equation (1) and ignore the "Self-Propelled" aspect of the SPV model. We simulate a tissue containing  $N$  cells under periodic boundary conditions with box size  $L \times L$  and set the parameters  $K_A = 1, K_P = 1$ . The homeostatically preferred cell area is set to be consistent with the average area per cell, i.e.  $A_0 = L^2/N$  and  $\sqrt{A_0}$  is used as the unit of length throughout this work. The preferred cell perimeter is rescaled  $p_0 = P_0/\sqrt{A_0}$  and varied between 3.7 and 4.6 [15]. Initially, cell centers are randomly placed according to a Poisson point process and then evolved to minimize equation (1) using the L-BFGS method.

It has been shown that by changing the value of the preferred cell perimeter  $p_0$ , tissues undergo a solid-fluid transition [15]. This transition occurs at a critical value of  $p_0^* = 3.81$ . When  $p_0 < p_0^*$ , the tissue behaves as rigid solid with a finite shear modulus and there are finite energetic barriers for a cell to move or rearrange. Above  $p_0^*$ , the tissue becomes a fluid, with a vanishing shear modulus as well as vanishing energy barriers for rearrangements. Coupled to these mechanical changes is a clear signature in cell shapes at the transition [16, 22], the shape-based order parameter calculated by averaging the *observed* cell perimeter-to-area ratio  $s = \langle P/\sqrt{A} \rangle$  grows linearly with  $p_0$  when  $p_0 > p_0^*$  in the fluid phase but remains at a constant ( $s \approx p_0^*$ ) in the solid phase. Fig. 1(a) shows typical tissue snapshots generated using the SPV model. Geometrically, the SPV model ground states form amorphous tilings where the cells have approximately equal area, but varying perimeters as dictated by  $p_0$ . These predictions for cell shapes have been used successfully to determine the mechanical behavior of tissues in experiments [22].

In order to use the SPV model to design a photonic material, it is crucial to understand the structural properties of the cell centers. We first analyze the pair-correlation function  $g(r)$  of cell centers to probe short-range order.  $g(r)$  for the solid phase ( $p_0 < 3.81$ ) shows mutual exclusion between nearest neighbors (Fig. 2) and becomes constant at large  $r$ . These features are similar to those observed in other amorphous materials with short-range repulsion and lack of long range order, such as a jammed granular materials [23] or dense colloids arrays [24]. As  $p_0$  is increased and the tissue transitions into the fluid phase, the high preferred perimeters can only be satisfied if the cell shapes become more elongated. As a result, the cell centers can become arbitrarily close to each other with a  $g(r)$  that is reminiscent of an ideal gas in the limit of high  $p_0$ .

The structure factor  $S(q)$  at various  $p_0$  values are also shown in Figs. 1(b) and 2. The first striking behavior is that for all  $p_0$  values, the structure factor vanishes when  $q = 0$ , which corresponds to a persistent density correlation at large distances. While the behavior of  $\lim_{q \rightarrow 0} S(q) = 0$  naturally holds for a crystalline lattice, it is surprising to find it in an amorphous structure without translational order. In fact this type of hidden long range order is a characteristic of **hyperuniform** [13, 25] patterns. Briefly, a point pattern is hyperuniform if the variance of the number of points  $\sigma_R^2$  in an observation window of size  $R$  grows more slowly than the volume of the window. This is in contrast to the  $\sigma_R^2 \propto R^d$  scaling that typically holds for uncorrelated random point patterns. Indeed, we find that the distribution of cell centers in the SPV model are strongly hyperuniform (Fig. 3(a)), i.e. the number variance scales as the linear window size or  $\sigma_R^2 = \Lambda R/D$ . Here,  $\Lambda$  is the a surface constant that depends directly on the value of  $p_0$  and  $D = \sqrt{N/L^2} = 1$  is the average cell spacing. Furthermore, the value of  $\Lambda$  can be directly tuned by changing  $p_0$ . In the solid phase of the tissue ( $p_0 < p_0^*$ ),  $\Lambda \approx 0.5$  and stays constant as function of  $p_0$ . This is just slightly higher than the reference value reported [13] for the triangular lattice ( $\Lambda_{tri} \approx 0.4841$ ) and the square lattice ( $\Lambda_{sq} \approx 0.4576$ ). In the fluid phase  $\Lambda$  is tunable and proportional to  $p_0 - p_0^*$ .

It was recently suggested that strongly hyperuniform amorphous patterns can be used to design photonic materials that yield photonic bandgaps [7, 8]. Florescu & coworkers [7] further conjectured that the value of the surface constant constant between  $\Lambda$  should directly control the width of the bandgaps. We next take advantage of these design principles and create photonic materials based on SPV point patterns.

For any point pattern (crystalline or amorphous), the first necessary step in photonic design is to decorate it with materials that have a high dielectric contrast compared to the surrounding media. The simplest protocol is to just place cylinders centered at the each point  $\{\mathbf{r}_i = (x_i, y_i)\}$  that extends

infinitely in the  $z$ -direction. Such design typically yield band gaps in the Transverse Magnetic (TM) polarization (the magnetic field is parallel to the  $xy$ -plane) [26]. Based on this design, we first construct a material using SPV point patterns. In order to maximize the size of the band gap, the cylinders are endowed with dielectric constant of  $\epsilon = 11.56$  and radius  $r/D = 0.189$  [12]. The photonic band structure is calculated numerically using the plane wave expansion method [27] (see Methods). The TM band structure based on a SPV ground state at  $p_0 = 3.85$  is shown in Fig. 4(a). We also calculate the TM optical density of states (D.O.S.) for a large range of  $p_0$  values, shown in Fig. 4(b) and the TM gap-midgap ratio  $\Delta\omega/\omega_0$  is plotted as function of  $p_0$  in Fig. 5. This clearly shows that  $p_0$  not only tunes the mechanical response but simultaneously tunes the size of the PBG.

When the material behaves as a solid ( $p_0 < p_0^*$ ), it possesses the largest band gap with a  $\Delta\omega/\omega_0 \approx 0.36$  that plateaus as function of  $p_0$ . In the fluid phase ( $p_0 > p_0^*$ ),  $\Delta\omega/\omega_0$  decreases as  $p_0$  increases, yet stays large and finite in the range of  $3.81 < p_0 < 4.2$ . Since the fluid state has zero shear modulus and can rearrange due to external driving or thermal perturbations [15, 16], this gives rise to a **photonic liquid** where the PBG does not require a static and rigid structure.

To further demonstrate the robustness of the photonic fluid phase. We apply a finite temperature  $T = 0.006$  to a state at  $p_0 = 3.82$ . The material eventually fluidizes [16] as shown by the mean squared displacement of cell centers (inset of Fig. 4(c)). Remarkably, the TM PBG width stays constant in time as the material undergoes large scale rearrangements (Fig. 4(c)).

We also test a second method [7, 12] which yields complete PBGs, i.e. gaps in both TM and Transverse Electric (TE) polarizations. we use a design based on the Delaunay triangulation of the point pattern of the cell centers. Cylinders with  $\epsilon = 11.56$  and radius  $r/D = 0.18$  are placed at the nodes of the Delaunay triangulation while walls with  $\epsilon = 11.56$  and thickness  $w/D = 0.05$  are placed on the bounds of this trivalent network. Similarly, the size of the complete gap can be tuned along side the mechanical property by changing  $p_0$  (Fig. 5).

We have introduced a new design for 2D amorphous material with a tunable PBG. It will be straight forward to manufacture static photonic materials based on this design using 3D printing or laser etching techniques [8, 11]. A even more exciting possibility is to adapt this design protocol to self-assemble structures. Recent advances in biomimetic emulsion droplets [28] and nanoparticles grafted with polymer brushes [29] make it possible to tune the effective tension of individual particles as well as the adhesion strengths between particles. This should be sufficient to mimic the interaction between cells and give rise to a controllable preferred cell perimeter. Whereas

3D printed materials have scattering units that are millimeters apart [8] and have PBGs in the microwave spectrum, emulsion droplets and nanoparticles will push the PBG towards the visible spectrum.

As the name suggests, the full SPV model contains cells that are self-propelled. It will be very interesting to explore the photonic properties of fully active systems. We have seen preliminary evidence that in the active fluid phase of the SPV model, the cells are still correlated with short-range order as well as hyperuniformity at long-ranges, which should again give rise to PBGs. Another interesting avenue for future work is to use the pattern formation of a mixture of active and non-active cells to design and self-assemble structures that will have non-conventional wave-guiding properties.

We showed that the SPV model gives rise to tunable hyperuniform patterns as function of  $p_0$ . At large values of  $p_0$ , the model shows patterns where short-range order is absent but still suppresses long-range density fluctuations strongly. However, we have shown that hyperuniformity is not sufficient for obtaining PBGs. Rather, the presence of short range order is crucial for a PBG. For the design presented here, it is clear that the band gaps disappear when the  $\lim_{r \rightarrow 0} g(r)$  becomes nonzero, at around  $p_0 = 4.2$  (Fig. 5), while the patterns remain hyperuniform at higher  $p_0$ , they negligible band gaps. This is consistent with a recent paper by Froufe-Pérez et al [12] which explored the role of short-range order and hyperuniformity in photonic materials based on hard sphere packings and the SHU protocol.

While the work here focus on 2D structures, the SPV model can be easily extended to 3D. The energy functional equation (1) can be generalized to 3D by replacing the cell area with 3D cell volume and the perimeter with surface area [30]. These structures should also have full PBG since they are hyperuniform and have tunable short-range order. It will be an interesting direction for future research.

## METHODS

### Characterization of Structure

The structure factor is given by

$$S(\mathbf{q}) = \left\langle \frac{1}{N} \sum_{j,k}^N e^{i\mathbf{q} \cdot (\mathbf{r}_j - \mathbf{r}_k)} \right\rangle, \quad (2)$$

where  $N$  is the number of cells.  $\langle \dots \rangle$  averages over 200 SPV ground state configurations. Configurations containing 400 cells are used for this calculation.

To characterize hyperuniformity, the number of cells contained within an observation window of radius  $R$  and centered at  $\mathbf{r}_0$  is then calculated using

$$N_R = \int_{|\mathbf{r}-\mathbf{r}_0|<R} \rho(\mathbf{r}) d\mathbf{r}, \quad (3)$$

where  $\rho(\mathbf{r}) = \sum_{i=1}^M \delta(\mathbf{r} - \mathbf{r}_i)$  is the number density. The cell number variance is then given by

$$\sigma_R^2 = \langle N_R^2 \rangle - \langle N_R \rangle^2. \quad (4)$$

Here  $\langle \dots \rangle$  averages over random window center positions  $\mathbf{r}_0$  and 200 SPV ground state configurations at each  $p_0$ . Configurations containing 400 cells are used for this calculation.

### Calculation of Photonic Properties

All photonic properties are calculated using the MIT Photonic Bands program [27] under the supercell approximation, i.e. a finite sample of 64 cells is repeated periodically. The photonic band structure is calculated by following the conventional path of  $\Gamma = (0,0) \rightarrow M = (1/2, 1/2) \rightarrow K = (-1/3, 1/3) \rightarrow \Gamma$  in reciprocal space. The optical density of states at each value of  $p_0$  is calculated by tabulating eigenfrequencies from 10 samples.

### ACKNOWLEDGMENTS

The author wishes to thank M. Lisa Manning, who was instrumental in inspiring this work. She brought the author into the field of tissue mechanics and first suggested that tissue morphologies may be naturally hyperuniform. The author acknowledges the support of the Raymond and Beverly Sackler Fellowship and the Center for Studies in Physics and Biology at Rockefeller University. The author also acknowledges the High Performance Computing Cluster at Northeastern University.

---

[1] Sajeed John, “Strong localization of photons in certain disordered dielectric superlattices,” Phys. Rev. Lett. **58**, 2486–2489 (1987).

- [2] Eli Yablonovitch, “Inhibited spontaneous emission in solid-state physics and electronics,” *Phys. Rev. Lett.* **58**, 2059–2062 (1987).
- [3] Hui Cao, “Random lasers: Development, features and applications,” *Opt. Photon. News* **16**, 24–29 (2005).
- [4] Alongkarn Chutinan, Sajeev John, and Ovidiu Toader, “Diffractionless flow of light in all-optical microchips,” *Phys. Rev. Lett.* **90**, 123901 (2003).
- [5] Diederik S. Wiersma, “Disordered photonics,” *Nat Photon* **7**, 188–196 (2013).
- [6] Lei Shi, Yafeng Zhang, Biqin Dong, Tianrong Zhan, Xiaohan Liu, and Jian Zi, “Amorphous photonic crystals with only short-range order,” *Advanced Materials* **25**, 5314–5320 (2013).
- [7] Marian Florescu, Salvatore Torquato, and Paul J. Steinhardt, “Designer disordered materials with large, complete photonic band gaps,” *Proceedings of the National Academy of Sciences* **106**, 20658–20663 (2009).
- [8] Weining Man, Marian Florescu, Eric Paul Williamson, Yingquan He, Seyed Reza Hashemizad, Brian Y. C. Leung, Devin Robert Liner, Salvatore Torquato, Paul M. Chaikin, and Paul J. Steinhardt, “Isotropic band gaps and freeform waveguides observed in hyperuniform disordered photonic solids,” *Proceedings of the National Academy of Sciences* **110**, 15886–15891 (2013).
- [9] Jin-Kyu Yang, Carl Schreck, Heeso Noh, Seng-Fatt Liew, Mikhael I. Guy, Corey S. O’Hern, and Hui Cao, “Photonic-band-gap effects in two-dimensional polycrystalline and amorphous structures,” *Phys. Rev. A* **82**, 053838 (2010).
- [10] Gaurasundar M. Conley, Matteo Burrelli, Filippo Pratesi, Kevin Vynck, and Diederik S. Wiersma, “Light transport and localization in two-dimensional correlated disorder,” *Phys. Rev. Lett.* **112**, 143901 (2014).
- [11] Nicolas Muller, Jakub Haberko, Catherine Marichy, and Frank Scheffold, “Silicon hyperuniform disordered photonic materials with a pronounced gap in the shortwave infrared,” *Advanced Optical Materials* **2**, 115–119 (2014).
- [12] Luis S. Froufe-Pérez, Michael Engel, Pablo F. Damasceno, Nicolas Muller, Jakub Haberko, Sharon C. Glotzer, and Frank Scheffold, “Role of short-range order and hyperuniformity in the formation of band gaps in disordered photonic materials,” *Phys. Rev. Lett.* **117**, 053902 (2016).
- [13] Salvatore Torquato and Frank H. Stillinger, “Local density fluctuations, hyperuniformity, and order metrics,” *Phys. Rev. E* **68**, 041113 (2003).



- [14] Tatsuzo Nagai and Hisao Honda, “A dynamic cell model for the formation of epithelial tissues,” *Philosophical Magazine Part B* **81**, 699–719 (2001).
- [15] Dapeng Bi, J. H. Lopez, J. M. Schwarz, and M. Lisa Manning, “A density-independent rigidity transition in biological tissues,” *Nat Phys* **11**, 1074–1079 (2015).
- [16] Dapeng Bi, Xingbo Yang, M. Cristina Marchetti, and M. Lisa Manning, “Motility-driven glass and jamming transitions in biological tissues,” *Phys. Rev. X* **6**, 021011 (2016).
- [17] Lars Hufnagel, Aurelio A. Teleman, H. Rouault, Stephen M. Cohen, and Boris I. Shraiman, “On the mechanism of wing size determination in fly development,” *Proceedings of the National Academy of Sciences* **104**, 3835–3840 (2007).
- [18] Reza Farhadifar, Jens-Christian Roper, Benoit Aigouy, Suzanne Eaton, and Frank Julicher, “The influence of cell mechanics, cell-cell interactions, and proliferation on epithelial packing,” *Current Biology* **17**, 2095 – 2104 (2007).
- [19] D. B Staple, R Farhadifar, J. C Roper, B Aigouy, S Eaton, and F Julicher, “Mechanics and remodelling of cell packings in epithelia,” *Eur. Phys. J. E* **33**, 117–127 (2010).
- [20] Alexander G. Fletcher, Miriam Osterfield, Ruth E. Baker, and Stanislav Y. Shvartsman, “Vertex models of epithelial morphogenesis,” *Biophysical Journal*, *Biophysical Journal* **106**, 2291–2304 (2014).
- [21] Dapeng Bi, Jorge H. Lopez, J. M. Schwarz, and M. Lisa Manning, “Energy barriers and cell migration in densely packed tissues,” *Soft Matter* **10**, 1885–1890 (2014).
- [22] Jin-Ah Park, Jae Hun Kim, Dapeng Bi, Jennifer A. Mitchel, Nader Taheri Qazvini, Kelan Tantisira, Chan Young Park, Maureen McGill, Sae-Hoon Kim, Bomi Gweon, Jacob Notbohm, Robert Steward Jr, Stephanie Burger, Scott H. Randell, Alvin T. Kho, Dhananjay T. Tambe, Corey Hardin, Stephanie A. Shore, Elliot Israel, David A. Weitz, Daniel J. Tschumperlin, Elizabeth P. Henske, Scott T. Weiss, M. Lisa Manning, James P. Butler, Jeffrey M. Drazen, and Jeffrey J. Fredberg, “Unjamming and cell shape in the asthmatic airway epithelium,” *Nat Mater* **14**, 1040–1048 (2015).
- [23] Corey S. O’Hern, Leonardo E. Silbert, Andrea J. Liu, and Sidney R. Nagel, “Jamming at zero temperature and zero applied stress: The epitome of disorder,” *Phys. Rev. E* **68**, 011306 (2003).
- [24] Willem K. Kegel, van Blaaderen, and Alfons, “Direct observation of dynamical heterogeneities in colloidal hard-sphere suspensions,” *Science* **287**, 290–293 (2000).
- [25] Chase E Zachary and Salvatore Torquato, “Hyperuniformity in point patterns and two-phase random heterogeneous media,” *Journal of Statistical Mechanics: Theory and Experiment* **2009**, P12015 (2009).

- [26] John D Joannopoulos, Steven G Johnson, Joshua N Winn, and Robert D Meade, *Photonic crystals: molding the flow of light* (Princeton university press, 2011).
- [27] Steven G. Johnson and J. D. Joannopoulos, “Block-iterative frequency-domain methods for maxwell’s equations in a planewave basis,” *Opt. Express* **8**, 173–190 (2001).
- [28] Lea-Laetitia Pontani, Ivane Jorjadze, Virgile Viasnoff, and Jasna Brujic, “Biomimetic emulsions reveal the effect of mechanical forces on cell–cell adhesion,” *Proceedings of the National Academy of Sciences* **109**, 9839–9844 (2012).
- [29] Sanat K. Kumar, Nicolas Jouault, Brian Benicewicz, and Tony Neely, “Nanocomposites with polymer grafted nanoparticles,” *Macromolecules* **46**, 3199–3214 (2013).
- [30] Matthias Merkel and M. Lisa Manning, “Unpubsihed,” (2016).

## FIGURES

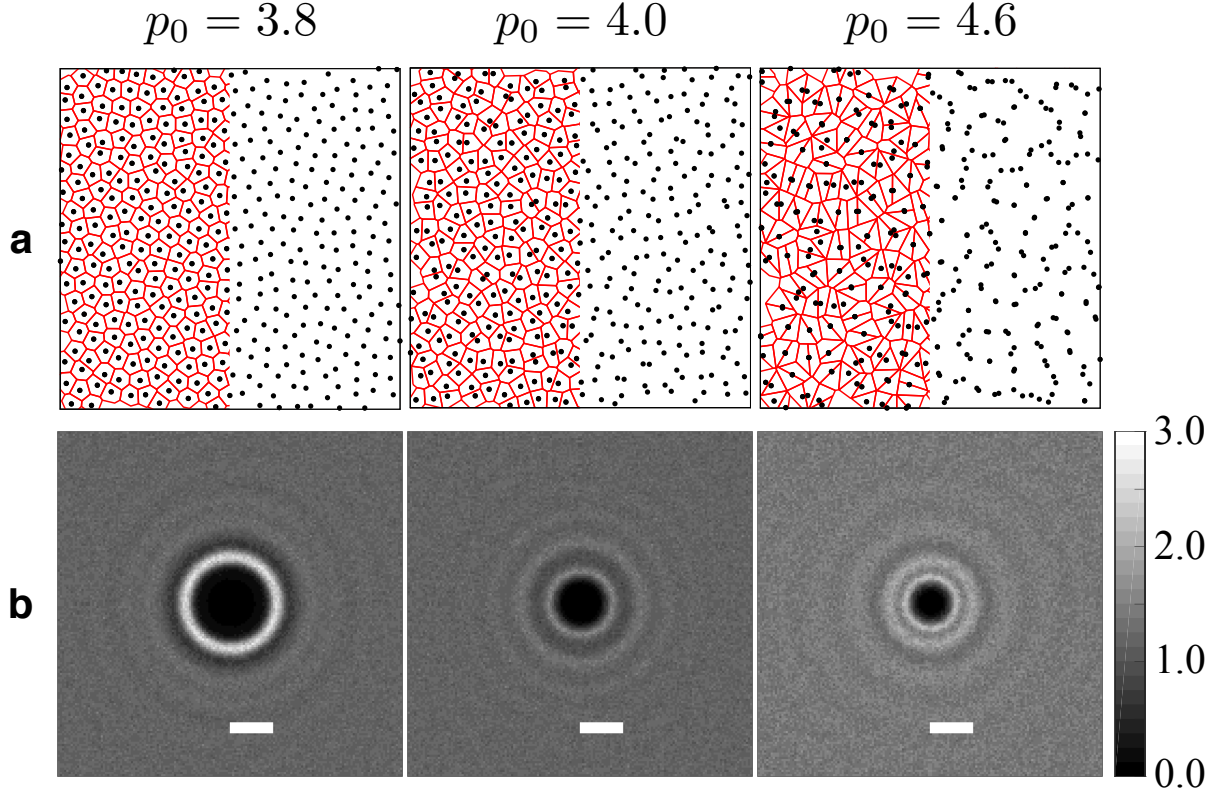


FIG. 1. **Tissue structure in the SPV model** (a) Simulation snapshots at 3 different values of the preferred cell perimeters  $p_0$ . Cell centers are indicated by points and cell shapes are given by their Voronoi tessellation. Model tissues containing 400 cells are shown. (b) Contour plot of the structure factor  $S(q_x, q_y)$  (see Methods) corresponding to the states shown in (a). Scale bar has length  $2\pi/D$  in reciprocal space, where  $D$  is the average spacing between cell centers.

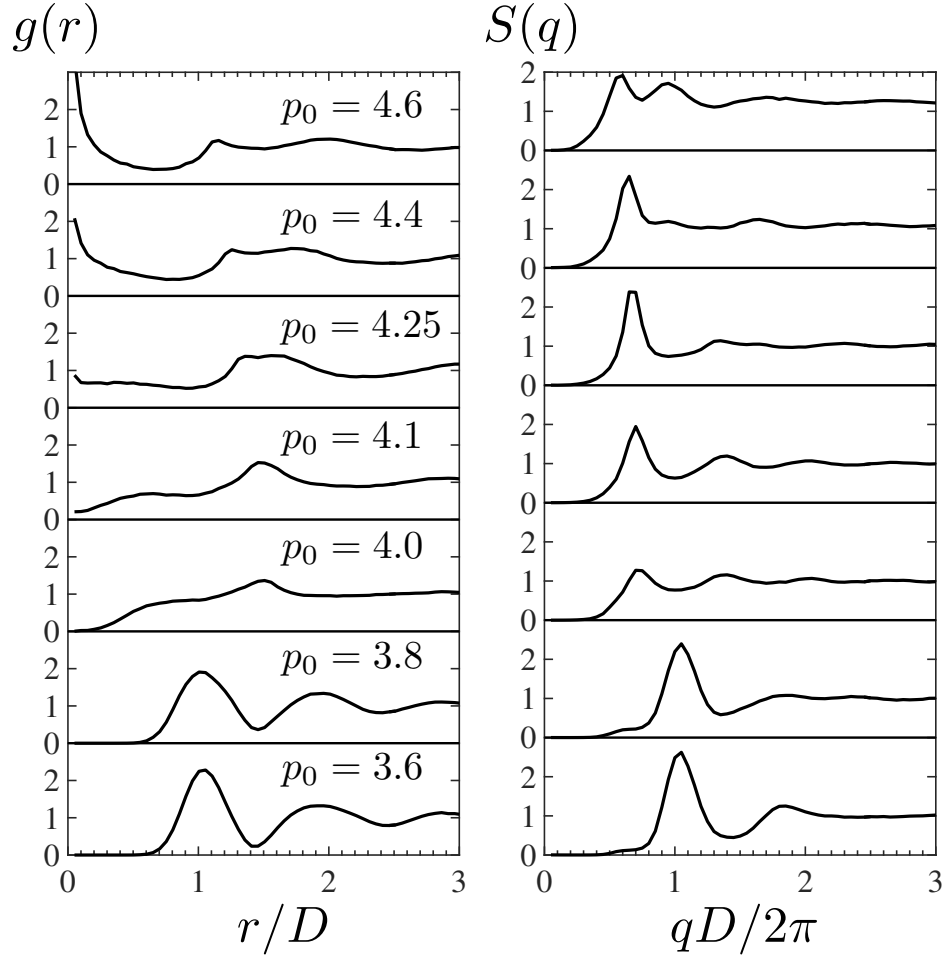
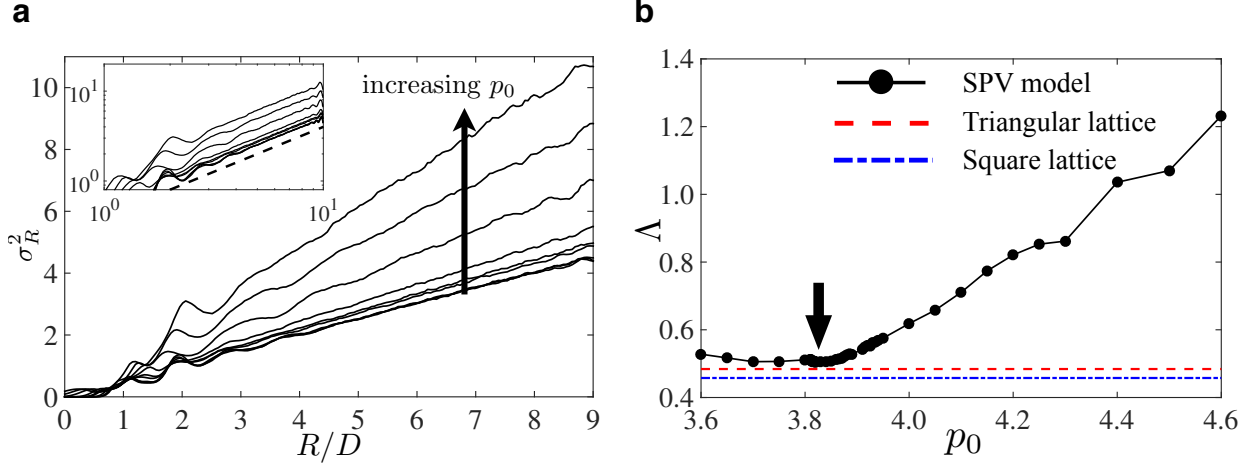


FIG. 2. **Tunability of Tissue Structure.** Pair-correlation function  $g(r)$  and the structure factor  $S(q)$  at different values of  $p_0$ .



**FIG. 3. Unusual density fluctuations and hyperuniformity in the SPV model.** (a) The cell number variation  $\sigma_R^2$  is linearly proportional to the observation window size  $R$  at various values of  $p_0$ . Different lines correspond to  $p_0 = 3.25, 3.35, 3.813, 3.83, 3.87, 3.89, 3.93, 3.94, 4.5$ . Measurements are averaged over 200 samples of tissues with  $N = 400$  cells as well as over randomly placed observation windows (see Methods). Inset shows the same data on a log plot, with the dashed line representing a slope of 1. (b) The constant of proportionality  $\Lambda$  between  $\sigma_R^2$  and  $R$  can be plotted as a function of  $p_0$ . The black arrow indicates the location of the solid-fluid transition for tissues ( $p_0 = 3.81$ ). The tissue behaves as a solid for  $p_0 > 3.81$ , and a fluid for  $p_0 < 3.81$ . Values corresponding to  $\Lambda$  in crystalline structures are given by the dashed lines.

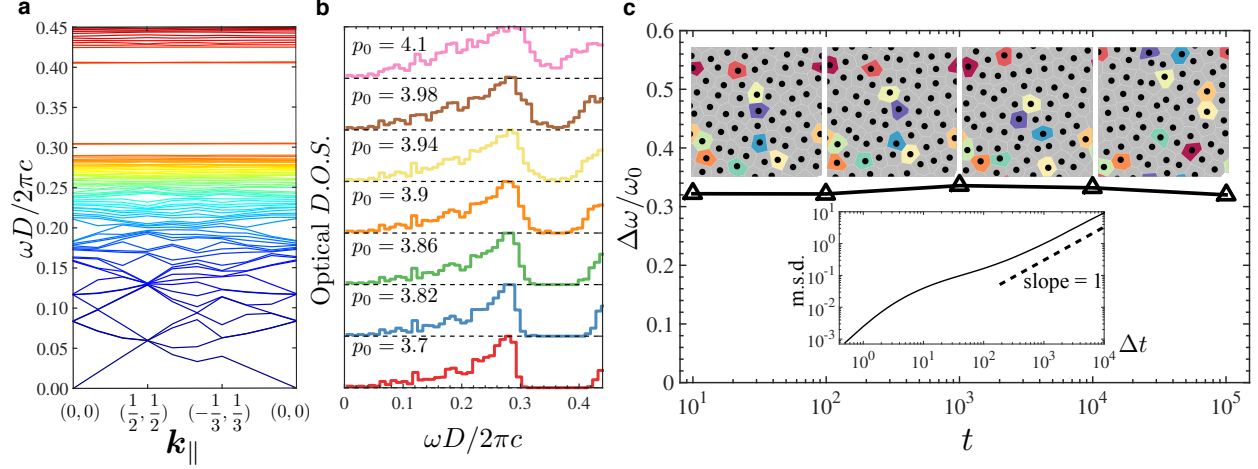


FIG. 4. **Photonic metamaterial based on the SPV model.** (a) Photonic band structure (TM) for the material constructed by placing dielectric cylinders at the cell centers exhibits a PBG. Design is based on a ground state of SPV at  $p_0 = 3.85$ .  $\mathbf{k}_{\parallel}$  is the in-plane wave vector. (b) The TM optical density of states at different values of  $p_0$ . (c) The TM gap-midgap ratio at  $p_0 = 3.82$  and finite temperature plotted at different times spanning 4 decades. The mean-square-displacement (m.s.d.) shows that the material fluidizes with a structural relaxation time of  $t \sim 10^3$ . The snapshots are taken at  $t = 10, 10^2, 10^3, 10^4$ . Here, 10 cells are tracked with colors to show structural rearrangements.

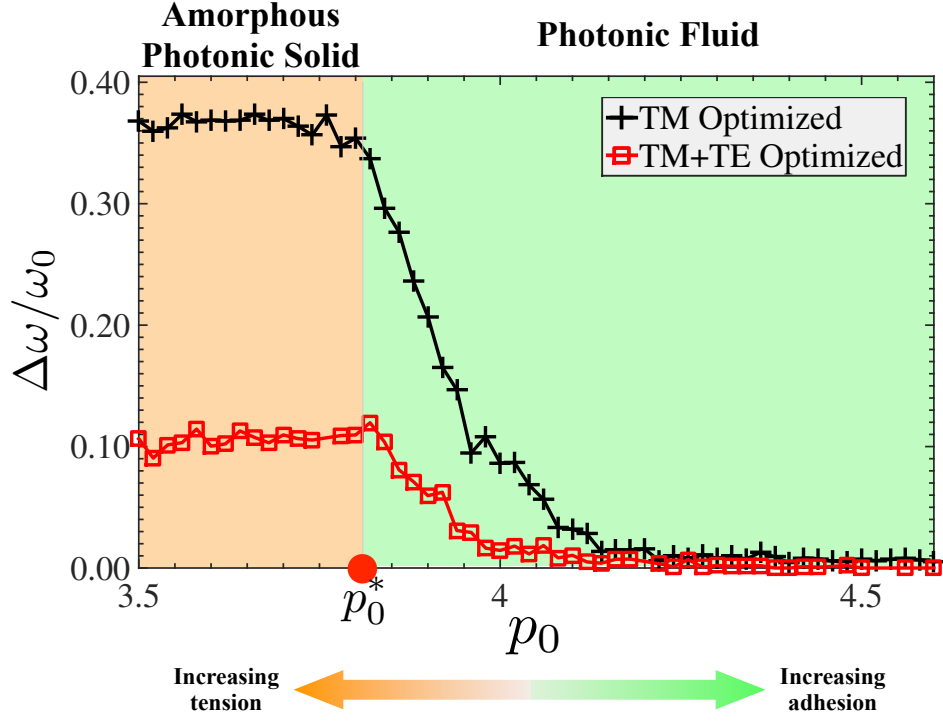


FIG. 5. The size of the photonic bandgap as function of  $p_0$ . "TM Optimized" corresponds to the size of the TM band gap for a material constructed by placing dielectric cylinders at cell centers. "TM+TE Optimized" corresponds complete PBG for a material constructed using a trivalent network design (see text). Phases are colored according to the mechanical property of the material. The red dot at  $p_0^* = 3.81$  corresponds to the critical point of the solid-fluid transition.